CJC Chinese Journal of Chemistry 中国化学 - An International Journal

For submission: https://mc.manuscriptcentral.com/cjoc
For published articles: https://onlinelibrary.wiley.com/journal/16147065

Concise Report

Cite this paper: *Chin. J. Chem.* **2023**, *41*, 1198—1208. **DOI: 10.1002/cjoc.202200754**

Two Dimensional Triptycene End-Capping and Its Influence on the Self-Assembly of Quinoxalinophenanthrophenazines†

Lisa Roß,[a] Julius Reitemeier,[a] Farhad Ghalami,[b] Wen-Shan Zhang,[c] Jürgen H. Gross,[a] Frank Rominger,[a] Sven M. Elbert,[a] Rasmus Schröder,[c] Marcus Elstner,[b] and Michael Mastalerz*[,a]

[a] *Institute of Organic Chemistry, Heidelberg University, Im Neuenheimer Feld 270, D-69120, Heidelberg, Germany*
[b] *Institute of Physical Chemistry and Theoretical Chemical Chemistry, Karlsruhe Institute of Technology, Kaiserstraße 12, D-76131, Karlsruhe, Germany*
[c] *BioQuant, University Heidelberg, Im Neuenheimer Feld 267, D-69120, Heidelberg, Germany*

Keywords

Triptycene | Quinoxalinophenanthrophenazine | *N*-Heteropolycycles | Polycyclic aromatic compounds | Aggregation

Comprehensive Summary

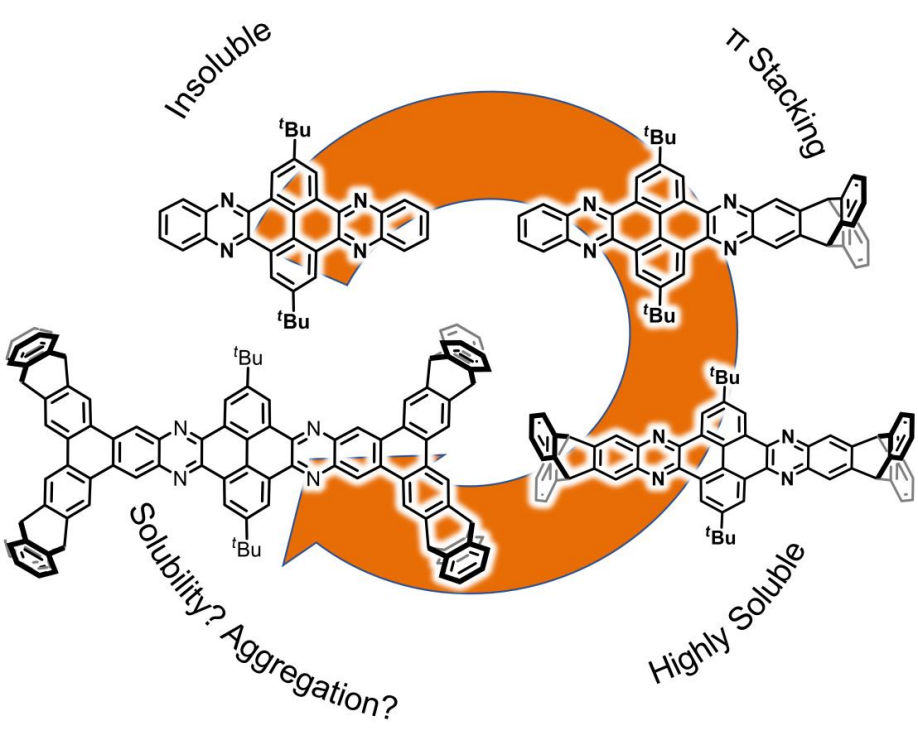

In this report we investigated two-dimensionally triptycene end-capped QPPs in terms of their solution and solid-state behavior. For this purpose, a triphenylene based *ortho*-diamine decorated with two triptycenyl units as well as a phenylene diamine with two non-annulated triptycene units have been synthesized. Sequences of condensation reactions with a pyrene-based tetraketone and *ortho*-diamines yielded a series of QPPs and UV/Vis investigations of the corresponding compounds led to the conclusion, that the QPPs form dimers in solution, which was further supported by MALDI-TIMS-TOF-MS. Single-crystal X-ray analysis of the triply and quadruply triptycene end-capped QPPs furthermore showed short π-π-distances of 3.3—3.4 Å and a perfect shape match during the dimerization of the triply triptycenyl end-capped QPP making it possible synthon for crystal engineering.

*E-mail: michael.mastalerz@oci.uni-heidelberg.de
† Dedicated to the Special Issue of Optoelectronic Functional Materials.

Background and Originality Content

Polycyclic aromatic hydrocarbons as well as their *N*-heterocyclic analogues are of potential interest for applications as materials in optoelectronic devices.[1-2] Numerous fabrication techniques of such devices rely on solution processing which is causing an inherent dilemma during the design of suitable (especially larger) molecules.[3-6] While on the one hand, solubilizing side-chains have to be introduced to enable solution-based processing techniques, on the other hand these side-chains hinder the intermolecular interactions of the π-systems and thus often the electronic communication in some cases, although the latter is crucial for semiconducting devices based on small molecules.[7-8] Furthermore and consequently, the tendency of such molecules to form large crystalline aggregates is prohibited which limits in-depth analyses by single crystal X-ray diffraction analysis (SCXRD) as observed, *e.g.*, for a large number of molecules solubilized with long alkyl side-chains.[9-13]

During the study of a series of triptycene-based tris-quinoxalino phenanthrophenazines (tQPPs),[14] a derivative containing triptycene end-caps showed the by far highest solubility (183 mg/mL in $CHCl_3$) in comparison to other compounds with substituents such as methoxy or hexyl groups.[15-16] This higher solubility can be explained by a less efficient packing of the polycyclic aromatic backbone units (here QPPs). Nevertheless, the corresponding QPP crystallized from various solvents which sounds contradictory at first.[15] Taking advantage of the beneficial combination of the solubilizing effect and the crystallization behavior, a pyrene-fused *N*-heteroacene with eleven rectilinearly annulated aromatic rings and two triptycenyl end-caps was introduced,[17] showing a well-resolved ^{1}H NMR-spectrum at 298 K in $CDCl_3$ while the similar π-backbone with long dodecyloxy groups led to broad peaks in deuterated oDCB, even at elevated temperatures (373 K).[13] The general concept of using two triptycene end-caps to substantially increase solubility[18] was further applied to hexabenzoovalenes,[19-21] benzo- and naphtothienobenzothiophenes,[22] chiral bis(diazadibenzoanthracenes),[23] indigo dyes,[24] benzo-fused perylene oligomers,[25] thieno-fused coronene nanoribbons[26] or a nanobelt based cycloiptycene.[27] However, when only one triptycene end-cap is attached to QPPs, precise π-dimerization occurred in the solid state, mostly independent from further substituents at the backbone.[28-31] Especially the latter observation is interesting to finally develop a crystal engineering synthon for controlling the orientation of π-stacking.

Acenes or related compounds that contain triphenylenes at their peripheral ends are known to stabilize the π-backbones electronically.[32-36] The structural motif of triphenylenes allow the implementation of three or four triptycene end-caps to longer QPP derived poly *N*-heterocyclic aromatic compounds, which is introduced herein.[37-38]

Results and Discussion

Synthesis and characterization

To expand the triptycene end-capping of QPPs in two dimensions, the bis-triptycenyl diamine building block **5** was synthesized in three-steps starting with a Suzuki-Miyaura cross-coupling reaction of dibromo dinitro benzene **1**[39] and pinacol boronane **2**[38] to give **3** in 64% yield (Scheme 1). By oxidative cyclodehydration

Scheme 1 Synthesis of the QPP derivatives **10a**, **10b**, **12** and **13**

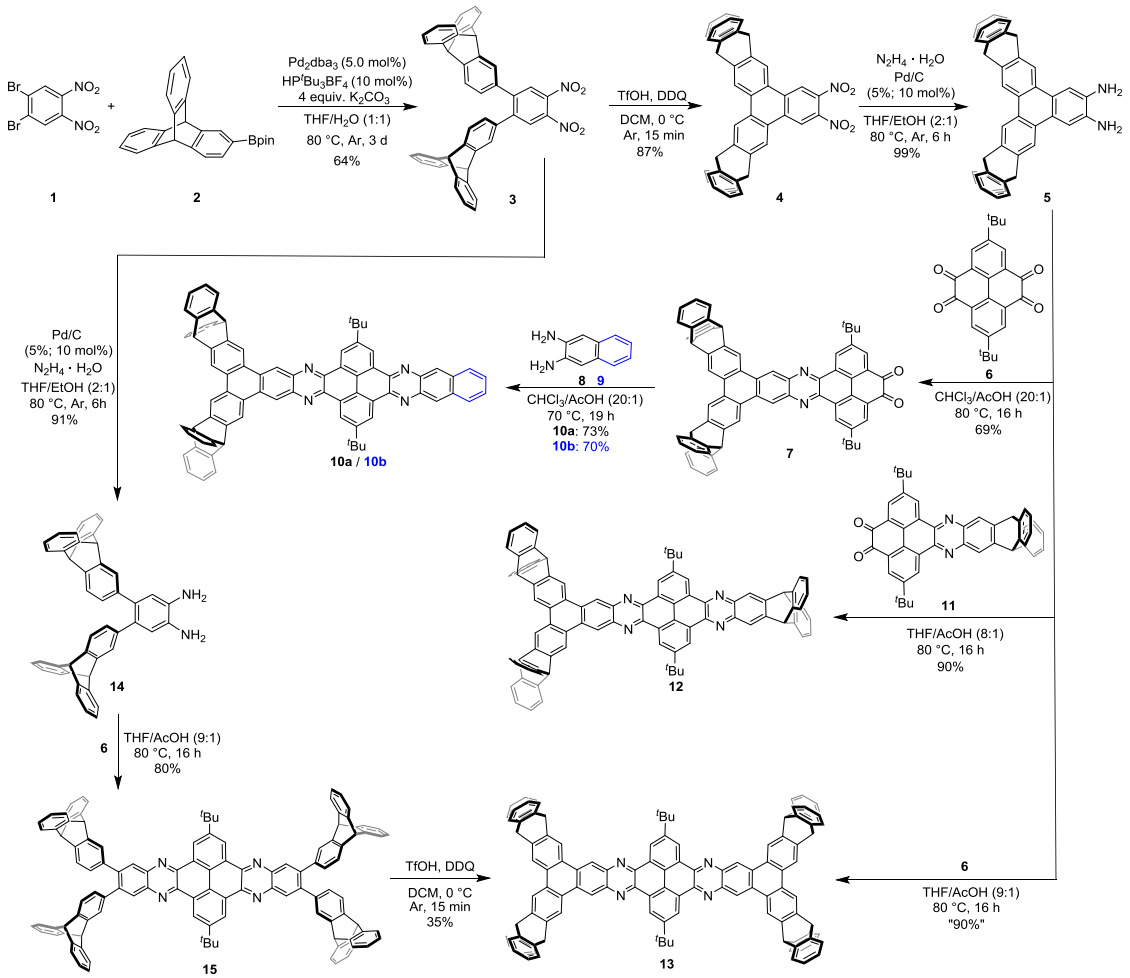

(DDQ, TfOH), triphenylene **4** was obtained in 87% yield selectively.[38] Finally, reduction with $N_2H_4{\cdot}H_2O$ and Pd/C (5%) gave the corresponding diamine **5** in a quantitative yield. All compounds were characterized by common analytical methods and **5** in addition by SCXRD (see Supporting Information).

With this in hand, π-extended dione **7** was synthesized by acid catalysed condensation of diamine **5** with an excess of pyrenetetraone **6**[40] in 69% yield.[14] The formation was confirmed by MALDI-mass spectrometry by a peak at *m/z* 948.3712 (calcd *m/z* 948.3716) as well as by NMR and IR spectroscopy (see Supporting Information). Subsequent condensation ($CHCl_3$/AcOH 20 : 1) with 1,2-phenylenediamine (**8**) or 2,3-naphthalenediamine (**9**) gave the corresponding QPPs **10a** in 73% and **10b** in 70% yield. These two derivatives which precipitated during the reaction, were collected by filtration and purified by washing. Both compounds show very poor solubility (for detailed discussions about the solubilities see sections below) in common organic solvents (DCM, $CHCl_3$, THF, oDCB, toluene) and thus could not be analysed by NMR spectroscopy. By LDI-mass spectrometry, the molecular ion peaks of **10a** (*m/z* 1020.4175, calcd: *m/z* 1020.4186) and **10b** (*m/z* 1070.4332, calcd: *m/z* 1070.4343) respectively were observed alongside clearly assignable fragmentation products (see Supporting Information). Furthermore, the absence of the N—H stretching bands of diamine **5** ($\tilde{\nu}$ = 3300—3000 cm^{-1})[41] as well as of the carbonyl stretching band of diketone **7** ($\tilde{\nu}$ = 1679 cm^{-1}) in the IR spectra of **10a** and **10b** (Figure 1) indicated full conversions and the corresponding C=N stretching modes were detected instead (**10a**: $\tilde{\nu}$ = 1610 cm^{-1}, **10b**: $\tilde{\nu}$ = 1610 cm^{-1}).

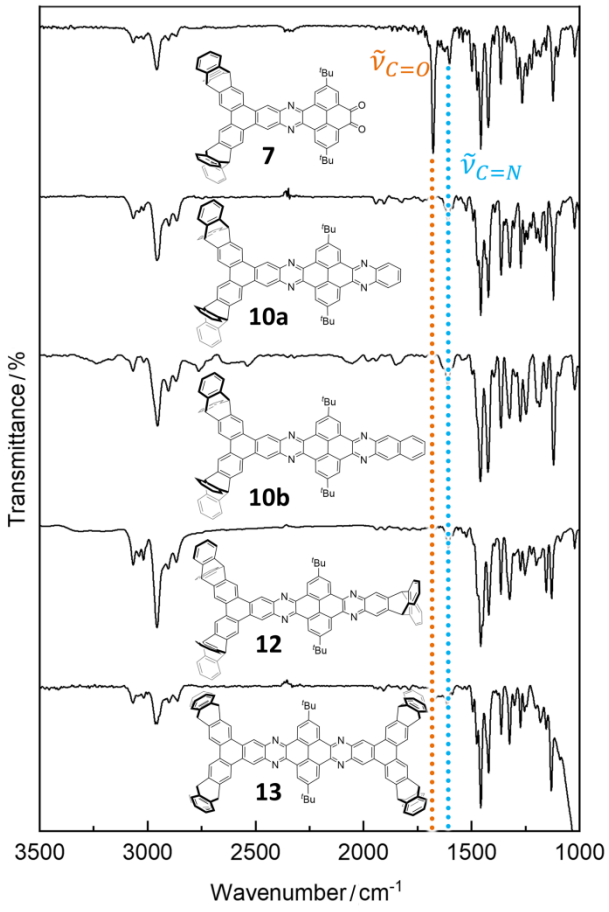

Figure 1 Comparison of the IR spectra (ATR, ZnSe) of the QPP derivatives **7**, **10a**, **10b**, **12** and **13.**

To increase the solubility, diamine **5** was reacted with triptycene end-capped diketone **11**[17] in THF and acetic acid (8 : 1) for 16 h at 80 °C and the triply triptycene end-capped QPP-derivative **12** was obtained in 90% yield (Scheme 1). In comparison to the phenyl- **10a** and naphthyl-derivatives **10b**, QPP **12** showed a higher solubility, but still it was insufficient for NMR-spectroscopic investigations. By MALDI-TOF mass spectrometry, the signal of the corresponding molecular ion of **12** at *m/z* 1196.4832 (calcd: *m/z* 1196.4818) was clearly detected (see Supporting Information). The condensation was also indicated by IR spectroscopy with a C=N stretching band at $\tilde{\nu}$ = 1609 cm^{-1} (Figure 1). Performing the reaction at room temperature with elongated reaction times (up to 14 d) led to the formation of crystals directly from the reaction mixture suitable for SCXRD analysis unambiguously proving the structure of **12** (see discussion below).

When diamine **5** was reacted with pyrene tetraketone **6**, but this time in a stoichiometric ratio of 2.2 : 1.0, QPP derivate **13** was obtained in about 90% (Scheme 1). Minor impurities were detected by ^{1}H NMR spectroscopy that we were not able to remove neither by washing, crystallization, column chromatography nor by size exclusion chromatography. Alternatively, a QPP core with flexible end-caps was synthesized first and the rigidification to **13** occurred in the final step. For this purpose, **3** was directly reduced ($N_2H_4{\cdot}H_2O$, Pd/C (5%)) to obtain the corresponding diamine derivative **14** in 91% yield (Scheme 1), which was condensed with pyrene tetraketone **6** (THF/AcOH (9 : 1)) to give tetra-triptycenyl QPP **15** in 80% yield. A final Scholl-type oxidative cyclodehydrogenation reaction (DDQ, TfOH) gave pure fourfold triptycene end-capped QPP **13** after recrystallization from THF albeit in lower yields of 35%. MALDI-TOF mass spectrometry confirmed the loss of four protons and the protonated molecular ion of **13** was found at *m/z* 1522.5913 (calcd *m/z* 1522.5914). ^{1}H NMR spectroscopy revealed the high symmetry of QPP **13** by only eight signals in the region of aromatic protons (Figure 2). The peaks of H^b (δ = 9.70), H^c (δ = 9.16) and H^d (δ = 9.70) are characteristic singlets of the triphenylene subunits. Finally, single crystals of **13** were obtained by a similar method as for QPP **12** combining diamine **5** and tetraketone **6** at room temperature for 14 d (see discussion below).

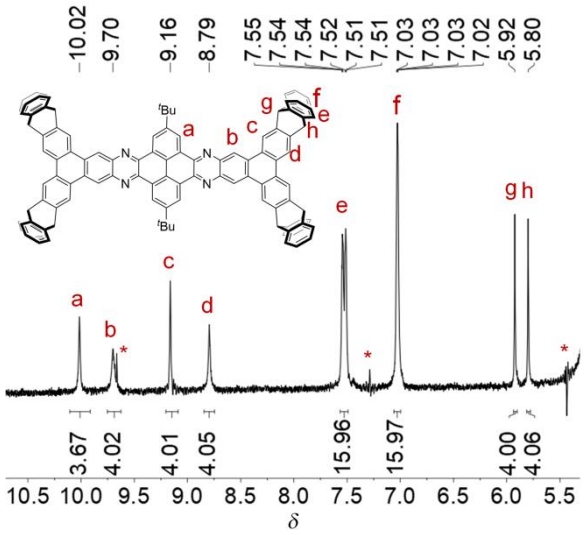

Figure 2 ^{1}H NMR spectrum (THF-d_8 + NaOD, 600 MHz, 295 K) of QPP **13**. $ marks satellites of THF-d_8, * marks residuals from the commercial THF-d_8 (proven by blank measurement). For the full spectrum, see Supporting Information.

Optoelectronic properties

The optical properties of the new QPP derivatives **10a**, **10b**, **12** and **13** have been investigated by UV/vis and fluorescence spectroscopy in DCM (Figure 3 and Table 1). All QPPs show most red-shifted absorption bands at approx. λ_{abs} = 460—467 nm. The bands of highest intensity (λ_{abs} = 350—359 nm) are at comparable wavelengths suggesting that the end-capped triptycenes have

only a small influence on absorption. This is further supported by fluorescence spectroscopy where for QPPs **10a**, **10b**, **12** and **13** two bands at λ_{em} = 492—494 nm and λ_{em} = 538—543 nm are found. In comparison to the parent *tert*-butyl and linearly triptycenyl end-capped QPPs (λ_{abs} = 414—420 nm),[28] QPP-based cruciforms (λ_{abs} = 414—438 nm),[42] QPPs with aromatic (λ_{abs} = 417—422 nm)[29] or electron donating substituents (λ_{abs} = 420 nm)[29] or even a tetracyano QPP (λ_{abs} = 440 nm),[43] the QPPs investigated in this study show a bathochromic shift of their lowest energy absorption bands. The most soluble derivative **15** (1.21 mmol/L in chloroform) possesses similar properties to the QPPs reported before (λ_{abs} = 438 nm; Figure 3 bottom) and its emission behavior is different from that of all other compounds of this series. This could be attributed to the formation of strong J-aggregates for **10a**, **10b**, **12** and **13** while **15** is present in the monomeric form due to its higher solubility. To further support this assumption, the most soluble QPPs **12** and **13** were investigated by UV/vis spectroscopy in various organic solvents ($CHCl_3$, THF, anisole, DCM, ODCB, isopropanol and acetonitrile) in a concentration range of 10^{-7}—10^{-4} mol/L and only negligible spectroscopic changes of max. $\Delta\lambda$ = 3 nm were observed (see Supporting Information). Additionally, drop casted films from DCM (Figure 3) showed only a small red-shift of $\Delta\lambda$ = 5—14 nm for all four investigated QPPs which is common in thin films.[44] This minor shift is most likely not attributed to further aggregation. Fluorescence microscopy of the crystalline samples shows a strong yellow fluorescence (Figure 3 insets), indicating once more the formation of J-aggregates, which is also supported by SCXRD (see below). In summary, all spectroscopic experiments strongly suggest the existence of the new QPPs as dimeric aggregates in solution at room temperature.

The QPP derivatives **10a**, **10b**, **12** and **13** were examined by cyclovoltammetry (CV) and differential pulse voltammetry (DPV) (see Supporting Information). Due to the low solubility, the measurements were performed as thin films prepared by drop-casting of saturated carbon disulfide solution of the respective QPPs onto the Pt-working electrode. For **10a** an irreversible reduction potential was observed at −1.81 V (which was confirmed by DPV).

QPP **10b** showed a reduction at −1.5 V with a second wave at −1.7 V. Similar first reduction potentials were also observed for QPP **12** (−1.7 V) as well as **13** (−1.6 V), yet in both cases more complex patters with four (**12**: −1.7 V, −2.1 V, −2.4 V and −2.7 V) and three (**13**: −1.8 V, −2.0 V and −2.6 V) reduction potential were evident (see Supporting Information). The corresponding electron affinities have been estimated to be between −2.8 eV (**10a**) and −3.2 eV (**10b**) (Table 1).

Mass spectrometric investigation of the aggregation behavior

For all synthesized QPPs, a favourable dimerization was found by mass spectroscopy. For QQPs **10a** and **10b**, the most effective MS technique was found to be LDI. In both cases, signals corresponding to dimeric species were found at *m/z* 2041.8371 for **10a** ([2M+H$^+$], calcd *m/z* 2041.8462) and *m/z* 2140.8676 for **10b** ([2M$^+$], calcd *m/z* 2140.8697). Attempts to increase the laser power to obtain a dissociation of the dimeric species was accompanied by the fragmentation of the molecules (as for example cleavage of *tert*-butyl groups). This was on the one hand preventing a detailed investigation of the interactions present but at the same time indicating a strong aggregation, since covalent bonds were broken prior to the cleavage of the dimers.

In the case of QPP **12**, a peak intensity for the corresponding dimer at *m/z* 2392.9693 (calcd *m/z* 2392.9630) was sufficient for tandem MS/MS experiments by MALDI-TOF-MS (Figure 4). After isolation of the ion [2M]$^+$, it was investigated by collision-induced dissociation (CID). The CID energy (also referred to as laboratory translational energy E_{lab}) can be understood as the energy a particle undergoes at an impact event in the drift chamber. This can give a rough estimate of the energy necessary for a dissociation of

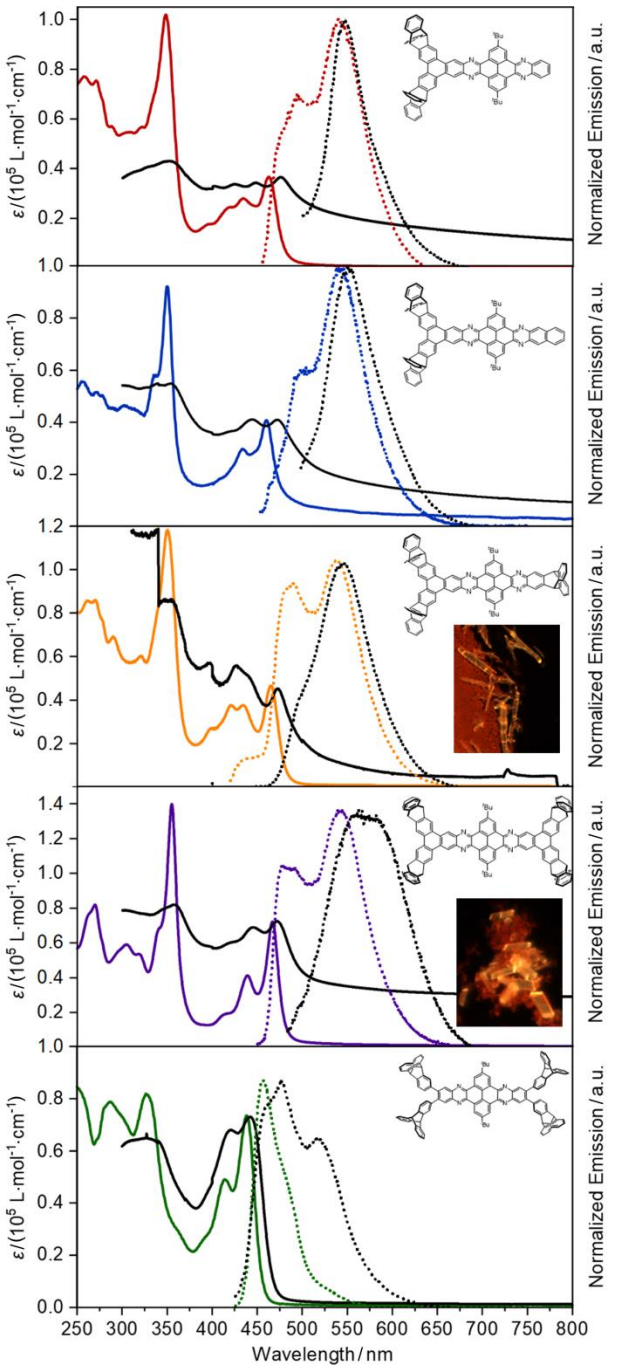

Figure 3 UV-Vis absorption (continuous lines) and normalized emission spectra (dashed lines) of **10a**, **10b**, **12**, **13** and **15** (top to bottom) in DCM solutions (colored spectra) and drop-casted (from DCM) films (black lines) at room temperature. The insets show fluorescence micrographs excited at 385 nm.

the dimer. The maximum energy E_{CM} by a collision partner (here N_2) can be calculated by the following equation:[45]

$$E_{CM} = E_{lab}\frac{m_{N_2}}{m_{N_2} + m_{molecule}}$$

At a CID energy of 10 V, dimeric QPP **12** was detected exclusively. Even at 50 V (55.8 kJ/mol), monomeric **12** was detected in only 1% relative intensity. At a maximum CID energy of 100 V, an 80 : 20 ratio of monomeric **12** to the corresponding dimer was observed which corresponds to a dissociation energy > 112 kJ/mol ($K_{diss} < 10^{-20}$) at room temperature.

In the case of quadruply triptycene end-capped QPP **13**, MALDI-TOF-MS experiments showed signals at *m/z* 3046.1868 (calcd *m/z*

Table 1 Optoelectronic properties of the QPP **10a**, **10b**, **12** and **13**

Compd	λ_{abs} [a,b]/nm	λ_{onset}/nm	λ_{em} [a]/nm	$\Delta\tilde{\nu}$/cm^{-1}	$E_{g(opt)}$/eV	$E_{red\,1}$ [d]/V	$E_{red\,2}$ [d]/V	$E_{red\,3}$ [d]/V	$E_{red\,4}$ [d]/V	IP [e]/eV	EA [e]/eV	$E_{HOMO,\,DFT}$ [f]/eV	$E_{LUMO,\,DFT}$ [f]/eV	$E_{g,\,DFT}$ [f]/eV
10a	462	480	543, 494	1402	2.6	−2.0*	—	—	—	−5.6	−2.8	−5.4	−2.3	3.1
10b	460	477	542, 501	1779	2.6	−1.6	−1.8	—	—	−5.9	−3.2	−5.4	−2.5	2.9
12	465	476	538, 492	1180	2.7	−1.7	−2.1	−2.4	−2.8	−5.8	−3.1	−5.6	−2.6	3.0
13	467	477	543, 479	536	2.6	−1.8	−1.8	−2.5	—	−5.8	−3.0	−5.6	−2.6	3.0

[a] Measured in DCM at room temperature. [b] Absorption maximum at the longest wavelength. [c] Estimated from onset $E_{g(opt)} = 1242/\lambda_{onset}$. [d] Reduction potentials derived from differential pulse voltammetry of films measured in acetonitrile or a saturated THF solution with Pt electrodes, Ag pseudo reference electrode and nBu$_4$NPF$_6$ as electrolyte. Scan speed 50 mV·s^{-1}; ferrocene/ferrocenium (Fc/Fc$^+$) was used as the internal reference. [e] $E_{LUMO} = -(E_{red,1} + 4.8)$ eV, $E_{HOMO} = E_{LUMO} - E_{g(opt)}$. [f] DFT calculated orbitals for the monomers (B3LYP/6–311(p,d)).

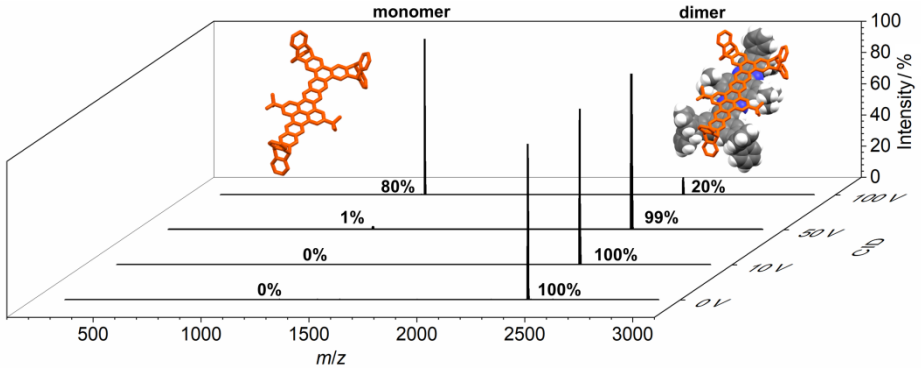

Figure 4 Tandem MS-MS experiments (MALDI-TIMS-TOF) of QPP **12** at various CID energies.

3046.1900) with low relative intensity corresponding to a dimeric aggregate. With increase of laser power, no dissociation was detected suggesting that here the interaction of π-stacking is even stronger than found for **12** .

Single crystal X-ray structures, transfer integrals and solubilities

QPPs **12** and **13** crystallized readily from the corresponding reaction mixtures resulting in single-crystals of sufficient quality for X-ray diffraction.

Triply end-capped QPP **12** crystallized in the triclinic space group $P\bar{1}$ with $Z = 2$ (Figure 5). The packing is dominated by the formation of π-π dimers of two adjacent molecules in an antiparallel fashion. These dimers form due to a favourable shape match of the *tert*-butyl groups, the three end-capping triptycenes and the QPP core. T-shaped π-π interactions between two triptycene units with $d_1 = 2.98$ Å as well as face-to-face interaction with $d_2 = 3.39$ Å are found (Figures 5a and 5b). The dimers pack in a crystallographically non-defined plane, again by T-shaped π-π interactions with $d_3 = 2.93$ Å and $d_4 = 2.91$ Å of the triptycenyl unit and additionally by dispersion interaction of the *tert*-butyl groups along the crystallographic *a*-axis (Figure 5e). Orthogonal to the π-planes of the dimers, electron density of disordered solvate molecules was found in the voids but needed to be removed by the SQUEEZE[46] routine function to solve the structure.

QPP **13** crystallizes also in the triclinic space group $P\bar{1}$ with $Z = 2$ (Figure 6) forming dimers. The *tert*-butyl groups, the QPP core and the four triptycene end-caps provide as well as in **12** a perfect match in shape. Here, the face-to-face π-π-interaction seems to be stronger, because the distance between the two π-planes is shorter ($d_1 = 3.36$ Å, Figure 6a). Due to the perfect shape matching, the dimeric alignment is slipped and the π backbones bend by 10° out of plane (Figure 6b). The π-stacked dimers show edge-to-face interactions ($d_2 = 2.86$ Å) of adjacent triptycene units with each other (Figure 6c) and create porous channels along the crystallographic *a*- and *b*-axis with diameters of $d_{p1a} = 4.3$ Å and $d_{p1b} = 17.2$ Å (Figure 6c). Perpendicular to that, a second type of pore with $d_{p2a} = 16.7$ Å and $d_{p1b} = 13.5$ Å was found (Figure 6e). Preliminary investigations by nitrogen sorption experiments on the crystalline and activated samples show that in principle, the pores can be made accessible for uptake of smaller compounds ($SA_{BET} = 77$ m^2/g for N_2 at 77 K). However, more detailed investigations on porosity are beyond the scope of this work and will be addressed in due course.

Because of the close packing of the dimers of QPPs **12** and **13**, we were interested in understanding electronic communication between two QPP units and calculated charge transfer integrals for hole and electron transport using the fragment orbital approach,[47] which has been implemented to the semi-empirical density functional tight-binding method (DFTB).[47-49] For triply end-capped QPP **12**, a high transfer integral of $t_{a,e} = 91$ meV for electrons and a lower one for holes ($t_{a,hole} = 16$ meV) were calculated (Table 2 and Figure 4). In the crystals, the aggregated dimers are electronically isolated resulting in the absence of further transfer integrals to the surrounding ($t_{a,e} = 0$ meV, $t_{a,hole} = 0$ meV). In the case of QPP **13**, the calculated charge transfer integrals ($t_{a,e} = 132$ meV, $t_{a,hole} = 88$ meV) were substantially bigger than for **12** (Table 2 and Figure 5). Again, the dimers are electronically isolated ($t_{b,e} = 0$ meV, $t_{b,hole} = 1$ meV; Figure 4).

Table 2 Selected solid state properties of the QPP **10a**, **10b**, **12** and **13** in comparison to QPPs published before

Compd.	Solubility[a]	Packing energy[b]	$d_{\pi\text{-}\pi}$ [c]	t_e [d]	t_h [d]
10a	0.078	—	—	—	—
10b	0.095	—	—	—	—
12	0.44	−366.5	3.39	91	16
13	0.36	−355.0	3.36	132	88
QPP[18,28]	0.25	−135.8	3.37	—	—
^{t}Bu-QPP[18,28]	0.97	−143.0	3.44	—	—
QPP-T[18,28]	—	−166.5	3.42	192	—
^{t}Bu-QPP-T[18,28]	—	−197.8	3.42	134	—
QPP-T$_2$[21]	1.3	−47.4	6.97	—	—
^{t}Bu-QPP-T$_2$[21]	11.5	−58.3	6.91	—	—

[a] Solubility in $CHCl_3$ in mmol/L. [b] Packing energy (in kJ/mol) between two QPPs calculated by the UNI force field method implemented in mercury.[50-51] [c] Distance (in Å) of two parallel QPP cores calculated from mean planes of 26 atoms of the six linearly annulated six-membered rings. [d] Transfer integrals (in meV) for electron (e) and hole (h) transport calculated by DFTB. For the structures of the literature known QPPs see Figure 7.

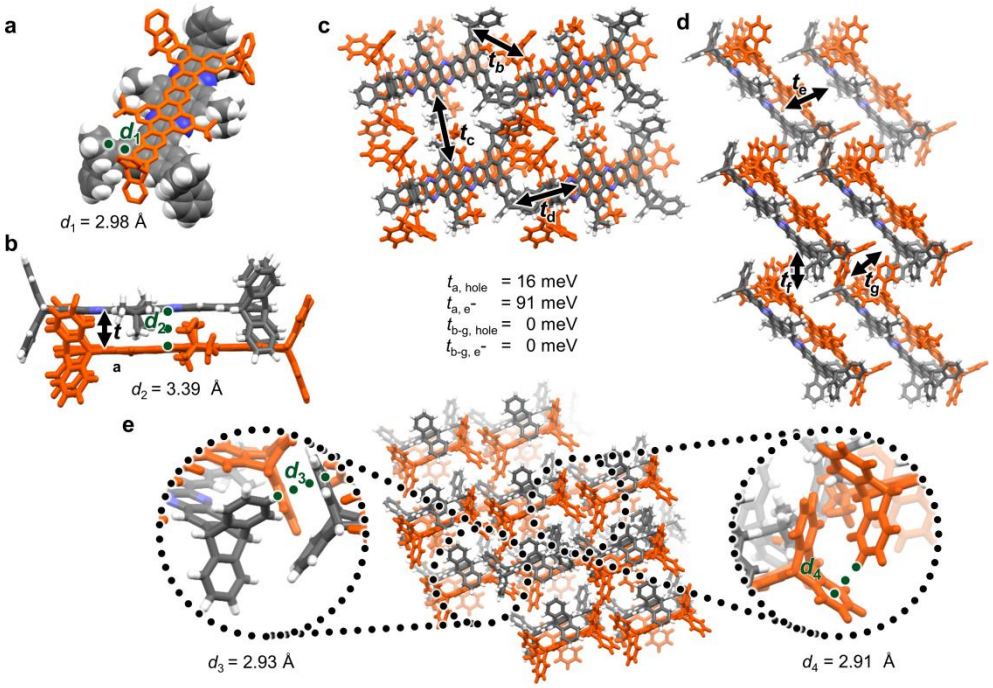

Figure 5 Single crystal X-ray structure of QPP **12**. a) and b) Dimeric alignments with edge-to-face π-π interactions (d_1) and face-to-face π-π interactions (d_2). c) Packing along the crystallographic *b*-axis. d) Packing along the crystallographic *a*-axis. e) Packing along a non-defined axis with zoom-ins on edge-to-face π-π-interactions (d_3, d_4). b) to d) Directions of calculated charge transfer integrals are shown as arrows.

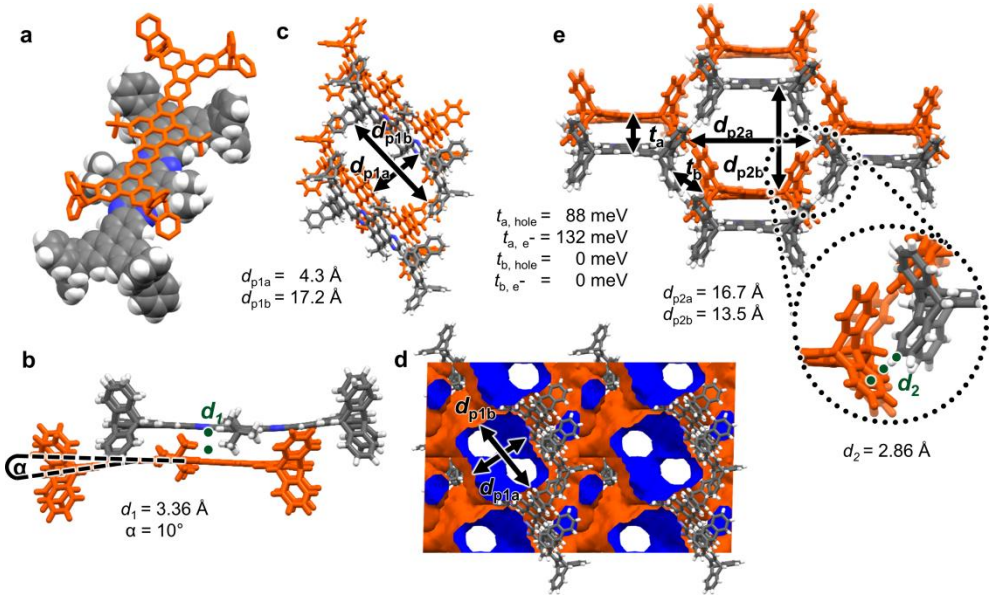

Figure 6 Single crystal X-ray structure of **13**. a) and b) Dimeric alignments with face-to-face π-π-interactions (d_1). c) Packing along the crystallographic b-axis. d) Packing along the crystallographic *b*-axis with crystalline voids represented as contact surface (orange: outer surface, blue: inner surface, created by Mercury 2020.1 with a probe radius of 1.82 Å and a grid spacing of 0.7 Å). e) Packing along a crystallographically non-defined axis with a zoom-in on the edge-to-face interactions between adjacent dimers (d_2). b) to d) Directions of calculated charge transfer integrals are shown as arrows.

All prior discussed findings show the strong formation of π-π dimers, which should decrease the solubility of such compounds (Table 2 and Figure 7). Indeed, **10a** (0.078 mmol/L) and **10b** (0.095 mmol/L) are 10—12 times less soluble in comparison to non-endcapped **^{t}Bu-QPP** (0.97 mmol/L) and still two to three times less than unsubstituted **QPP** (0.25 mmol/L). The addition of a second triptycene end-cap as in **12** and **13** increases the solubility 4.6—5.6 fold to 0.44 mmol/L (**12**) and 0.36 mmol/L (**13**). The higher aggregation tendency of the two-dimensional triptycene end-caps in comparison to the one-dimensional ones is most obvious comparing QPP **13** with **^{t}Bu-QPP-T$_2$**. In this case the 32 times lower solubility of **13** (0.36 mmol/L; **^{t}Bu-QPP-T$_2$**: 11.5 mmol/L) can be directly correlated to a hindered dimer formation in **^{t}Bu-QPP-T$_2$** ($d_{\pi\text{-}\pi}$ = 6.91 Å) while **13** forms close dimers with $d_{\pi\text{-}\pi}$ = 3.36 Å. The solubilities of two-dimensionally triptycene end-capped QPPs **12** and **13** can be found in the range of non-end capped **QPP** and **^{t}Bu-QPP** (Table 2), but at the same time their corresponding packing energies calculated by the UNI force field method implemented in the Mercury software package[50-51] are up to 2.7 times higher (**12**: −366.5 kJ/mol; **13**: −355.0 kJ/mol vs. **QPP**: −135.8 kJ/mol; **^{t}Bu-QPP**: −143.0 kJ/mol; Table 2). This is partly attributed to the larger systems.

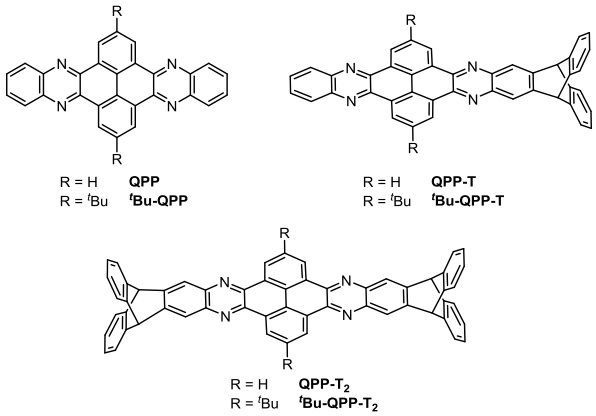

Figure 7 Molecular structures of the literature known QPPs listed in Table 2.

Conclusions

In summary, we explored how triptycene end-capping of triphenylene-based QPPs is influencing their tendency to form strong π-π dimers. All analytical tools at hand (solubility, UV/vis, MS and SCXRD) showed that all triphenylene-based QPPs with two, three or four triptycene end-caps show strong interactions and thus very low solubilities. Despite that, we were able to grow high-quality single-crystals of **12** and **13** direct from the reaction media. In both cases, dimers with relatively short distances of the π-planes were found, which can be explained by the nearly perfect self-matching shapes of the molecular structures. Especially their self-matching motif found for QPP **12** will now be further exploited to use it as a new and highly directing crystal-engineering synthon to make porous three-dimensional porous molecular materials,[14] capsules[52] and supracycles.

Experimental

General remarks

Deposition numbers 2216579 (**3**), 2216577 (**12**) and 2216578 (**13**) contain the supplementary crystallographic data for this paper. These data are provided free of charge by the joint Cambridge Crystallographic Data Centre and Fachinformationszentrum Karlsruhe.

Synthesis of 3

1,2-Dibromo-4,5-dinitrobenzene **1**[39] (147 mg, 450 µmol) and 2-triptycenylboronic acid pinacol ester **2**[38] (377 mg, 990 µmol, 2.2 equiv.) were stirred in an 8 mL screw cap vial for 30 min under an argon atmosphere. A solution of Pd_2dba_3 (21 mg, 22.5 µmol, 5 mol%) and $HP^tBu_3BF_4$ (15 mg, 50 µmol, 10 mol%) in degassed THF (1.5 mL) and a solution of K_2CO_3 (250 mg, 1.8 mmol) in degassed water (1.5 mL) were added. The reaction was stirred at 80 °C for 2 d. The mixture was cooled to rt and poured into water (2 mL) and extracted with DCM (3 × 4 mL). The combined organic layer was dried over $MgSO_4$, the solvent was removed under reduced pressure and the obtained crude solid purified by column chromatography (SiO_2, PE : EA, 10 : 1) to obtain **3** (195 mg, 290 µmol, 64%) as a yellow solid. m.p.: 377 °C dec. ^{1}H NMR (400 MHz, $CDCl_3$, 295 K): *δ*: 7.84 (s, 2H, H-2), 7.43—7.34 (m, 4H, H-13), 7.26—7.20 (m, 4H, H-10), 7.15 (d, *J* = 1.8 Hz, 2H, H-6), 7.06 (d, *J* = 7.8 Hz, 2H, H-17), 7.05—7.02 (m, 8H, H-11, H-12), 6.56 (dd, *J* = 7.6Hz, 1.8Hz, 2H, H-5), 5.35 (s, 2H, H-15), 5.16 (s, 2H, H-8). ^{13}C NMR (101 MHz, $CDCl_3$, 295 K) *δ*: 146.3 (2C, C-7/C-16), 146.3 (2C, C-7/C-16), 146.0 (2C, C-3), 144.9 (4C, C-9/C-14), 144.8 (4C, C-9/C-14), 141.4 (2C, C-1), 134.9 (2C, C-4), 127.1 (2C, C-2), 126.7 (2C, C-5), 125.5 (8C, C-11, C-12), 124.6 (2C, C-6), 123.9 (4C, C-10/C-13), 123.8 (4C, C-10/C-13), 123.7 (2C, C-17), 54.0 (2C, C-8), 53.9 (2C, C-15). IR (neat, ATR) $\tilde{\nu}$: 3063 (vw), 3036 (vw), 2959 (vw), 1597 (vw), 1537 (m), 1460 (w), 1427 (vw), 1360 (m), 1344 (w), 1256 (vw), 1192 (w), 1157 (w), 1121 (vw), 1022 (vw), 943 (vw), 918 (w), 885 (w), 851 (w), 833 (w), 806 (vw), 791 (w), 746 (vs), 665 (w), 627 (m) cm^{-1}. UV/VIS (DCM) λ_{abs} (lg *ε*): 350 (3.98), 278 (4.41), 271 (4.39) nm. Fluorescence (DCM) λ_{em} (λ_{ex}): 558, 451 (342) nm. HRMS (MALDI-TOF+, DCTB): *m*/*z* calcd for $C_{46}H_{28}N_2O_4$ [M]$^+$: 672.2044; found 672.2038. Elemental analysis: calcd (%) for $C_{46}H_{28}N_2O_4$·0.2 CH_2Cl_2: C 80.45, H 4.12, N 4.06. Found: C 80.38, H 4.17, N 3.94.

Synthesis of 4

Dinitro compound **3** (679 mg, 1.0 mmol) was dissolved in DCM (300 mL) under argon atmosphere. After cooling to 0 °C trifluoromethanesulfonic acid (3.0 mL) was added, resulting in a dark red solution. DDQ (363 mg, 1.6 mmol, 1.6 equiv.) was added in one portion and the obtained dark green mixture was stirred at 0 °C for 15 min. The reaction mixture was poured into sat. $NaHCO_3$ (aq.; 600 mL) solution and was stirred for 2 h. The mixture was extracted with DCM (3 × 200 mL), the combined organic layer was washed with $NaOH_{aq}$ (1 mol/L, 2 × 400 mL), water (2 × 300 mL), and brine (1 × 500 mL) and was dried over $MgSO_4$. The solvent was removed under reduced pressure, the crude solid was suspended in methanol (100 mL) and treated with ultra-sound for 20 min. The solid was collected by filtration, washed with methanol (100 mL) and *n*-pentane (50 mL) to obtain after drying in vacuum **4** as a pale-yellow solid (583 mg, 869 µmol, 87%). m.p.: 377 °C dec. ^{1}H NMR (600 MHz, THF-d_8, 295 K) *δ*: 9.32 (s, 2H, H-2), 8.87 (s, 2H, H-17), 8.82 (s, 2H, H-6), 7.50—7.46 (m, 8H, H-10, H-13), 7.02—6.99 (m, 8H, H-11, H-12), 5.80 (s, 2H, H-8/15), 5.79 (s, 2H, H-8/15). ^{13}C NMR (151 MHz, THF-d_8, 295 K) *δ*: 148.4 (2C, C-7), 146.3 (2C, C-16), 145.9 (4C, C-9/14), 145.8 (4C, C-9/14), 141.6 (2C, C-1), 133.5 (2C, C-3), 130.5 (2C, C-5), 126.5 (4C, C-11/12), 126.4 (4C, C-11/12), 126.4 (2C, C-4), 124.9 (4C, C-10/11), 124.8 (4C, C-10/11), 122.5 (2C, C-2), 120.2 (2C, C-6), 119.4 (2C, C-17), 55.3 (2C, C-8/15), 54.8 (2C, C-8/15). IR (neat, ATR) $\tilde{\nu}$: 3069 (vw), 3020 (vw), 2959 (vw), 1666 (vw), 1626 (vw), 1605 (vw), 1587 (vw), 1533 (s), 1458 (m), 1425 (w), 1348 (m), 1296 (vw), 1259 (vw), 1223 (vw), 1190 (w), 1155 (w), 1096 (vw), 1022 (vw), 976 (vw), 939 (vw), 887 (m), 852 (w), 806 (w), 787 (vw), 743 (vs), 708 (vw), 663 (w), 627 (m) cm^{-1}. UV/VIS (DCM) λ_{abs} (lg *ε*): 385 (4.06), 336 (4.29), 303 (4.60), 292 (4.61), 276 (4.72), 270 (4.77), 260 (4.72) nm. Fluorescence (DCM) λ_{em} (λ_{ex}): 554 (374) nm. HRMS (MALDI-TOF+, DCTB): *m*/*z* calcd for $C_{46}H_{26}N_2O_4$ [M]$^+$: 670.1893; found 670.1888. Elemental analysis calcd (%) for $C_{46}H_{26}N_2O_4$·1.1 MeOH: C 80.13, H 4.34, N 3.97. Found: C 79.90, H 4.30, N 3.70.

Synthesis of 5

In an argon-purged and oven dried 25 mL two necked round bottom flask triphenylene **4** (419 mg, 620 µmol) was dissolved in a 2 : 1-mixture of dry THF (14 mL) and dry ethanol (6.8 mL). Palladium on charcoal (5 wt%, 134 mg, 62 µmol, 10 mol%) was added in one portion and the mixture was heated to 80 °C. Hydrazine monohydrate (240 µL, 250 mg, 496 µmol, 8.0 equiv.) was added dropwise and the mixture was stirred for 6 h. After cooling to room temperature, the solid was filtered off and the solvent was removed from the filtrate under reduced pressure. The crude brown solid was suspended in *n*-pentane, treated with ultra-sound for 20 min and the solid collected by filtration to obtain **5** as a pale pink solid (374 mg, 611 µmol, 99%). ^{1}H NMR (600 MHz, THF-d_8, 295 K) *δ*: 8.62 (s, 2H, H-23), 8.39 (s, 2H, H-6), 7.77 (s, 2H, H-2), 7.46—7.36 (m, 8H, H-10, H-13, H-17, H-20), 6.97—6.90 (m, 8H, H-11, H-12, H-18, H-19), 5.64 (s,2H, H-8), 5.57 (s, 2H, H-15), 4.32 (s, 4H, NH). ^{13}C NMR (151 MHz, THF-d_8, 295 K) *δ*: 146.7 (4C, C-14, C-21), 146.6 (4C, C-9, C-16), 143.8 (2C, C-7), 142.6 (2C, C-22), 137.7 (2C, C-1), 128.8 (2C, C-4), 127.0 (2C, C-5), 126.0 (4C, C-11/12/18/19), 125.9 (4C, C-11/12/18/19), 124.4 (8C, C-10, C-13, C-17, C-20), 124.2 (2C, C-3), 118.8 (2C, C-23), 118.1 (2C, C-6), 108.4 (2C, C-2), 55.4 (2C, C-15), 55.3 (2C, C-8). IR (neat, ATR) $\tilde{\nu}$:

3406 (w), 3339 (w), 3065 (w), 3038 (w), 3018 (w), 2953 (w), 1636 (w), 1626 (w), 1585 (w), 1541 (w), 1501 (w), 1474 (w), 1456 (m), 1433 (m), 1379 (w), 1283 (w), 1182 (w), 1167 (w), 1155 (w), 1022 (w), 879 (m), 856 (w), 818 (w), 802 (w), 783 (w), 743 (vs), 696 (m), 642 (m), 625 (s) cm^{-1}. UV/VIS (DCM) λ_{abs} (lg ε): 372 (3.59), 354 (3.75), 315 (4.37), 290 (4.81), 272 (4.60) nm. Fluorescence (DCM) λ_{em} (λ_{ex}): 305 (342) nm. HRMS (MALDI-TOF+, DCTB ($CHCl_3$)): *m/z* calcd for $C_{46}H_{30}N_2$ $[M]^+$: 610.2409; found 610.2440. Elemental analysis calcd (%) for $C_{46}H_{30}N_2$·0.8 DCM: C 82.82, H 4.69, N 4.13. Found: C 82.67, H 5.13, N 4.17.

Synthesis of 7

In a 20 mL screw-capped vial diamine **5** (244 mg, 400 μmol) and pyrenetetraone **6** (449 mg, 1.2 mmol, 3.0 equiv.) was purged with argon for 15 min. The mixture was dissolved in chloroform (10.0 mL). After acetic acid (0.5 mL) was added, the reaction mixture was stirred at 80 °C for 16 h. After cooling to room temperature, the reaction mixture was poured into methanol (20 mL). The precipitate was collected by filtration and was washed with methanol (2 × 10 mL) and *n*-pentane (10 mL) to obtain after drying in vacuum dione **7** as a bright orange solid (263 mg, 277 μmol, 69%). m.p.: 258—260 °C. ^{1}H NMR (600 MHz, $CDCl_3$, 295 K) δ: 9.79 (d, *J* = 2.2 Hz, 2H, H-9), 9.55 (s, 2H, H-12), 8.92 (s, 2H, H-15), 8.65 (d, *J* = 2.2 Hz, 2H, H-4), 8.63 (s, 2H, H-26), 7.54—7.48 (m, 8H, H-19, H-22), 7.10—7.05 (m, 8H, H-20, H-21), 5.77 (s, 2H, H-17), 5.70 (s, 2H, C-24), 1.65 (s, 18H, H-1). ^{13}C NMR (151 MHz, $CDCl_3$, 295 K) δ: 180.5 (2C, C-6), 152.7 (2C, C-3), 145.9 (2C, C-25), 144.8 (4C, C-18/C-23), 144.7 (4C, C-18/C-23), 144.5 (2C, C-16), 142.1 (2C, C-10), 140.3 (2C, C-11), 133.2 (2C, C-7/C-13/C-14/C-27), 130.8 (2C, C-8), 130.4 (2C, C-4), 130.3 (2C, C-5), 130.2 (2C, C-9), 128.7 (2C, C-7/C-13/C-14/C-27), 128.6 (2C, C-7/C-13/C-14/C-27), 126.9 (2C, C-7/C-13/C-14/C-27), 125.8 (4C, C-20/C-21), 125.7 (4C, C-20/C-21), 124.0 (8C, C-19, C-22), 123.0 (2C, C-12), 119.7 (2C, C-15), 118.7 (2C. C-26), 54.4 (2C, C-17), 54.2 (2C, C-14), 35.8 (2C, C-2), 31.5 (6C, C-1). IR (neat, ATR) $\tilde{\nu}$: 2959 (w), 1678 (m), 1603 (w), 1499 (w), 1475 (w), 1458 (m), 1423 (m), 1366 (w), 1286 (w), 1267 (w), 1242 (w), 1223 (w), 1124 (w), 906 (w), 878 (m), 744 (vs), 725 (m), 627 (s), 611 (m), 586 (w), 554 (m), 540 (m), 517 (m), 501 (m), 486 (s), 478 (m), 467 (m), 459 (m), 438 (s), 422 (vs), 407 (m) cm^{-1}. UV/VIS (DCM) λ_{abs} (lg ε): 448 (4.67), 424 (4.49), 348 (5.15), 332 (4.88), 301 (4.94), 268 (4.85) nm. HRMS (MALDI-TOF+, DCTB): *m/z* calcd for $C_{70}H_{48}N_2O_2$ $[M]^+$: 948.3716; found 948.3712. Elemental analysis calcd (%) for $C_{70}H_{48}N_2O_2$·2MeOH: C 85.35, H 5.57, N 2.76. Found: C 85.51, H 5.52, N 2.88.

Synthesis of 10a

In an argon purged 8 mL screw-capped vial extended dione **7** (71 mg, 75 μmol) and *o*-phenylene diamine **8** (12 mg, 113 μmol, 1.5 equiv.) were dissolved in chloroform (4.2 mL). After acetic acid (0.25 mL) was added, the reaction mixture was stirred at 70 °C for 19 h. After cooling to rt, the obtained precipitate was collected by filtration and was washed with chloroform (5 mL) and methanol (10 mL) to obtain **10a** as a bright yellow solid (56 mg, 54 μmol, 73%). m.p.: >400 °C. NMR: Due to the low solubility, investigations by NMR-techniques were not possible. IR (neat, ATR) $\tilde{\nu}$: 3067 (w), 3040 (vw), 3020 (vw), 2959 (w), 2901 (w), 2866 (w), 1610 (w), 1589 (vw), 1526 (vw), 1493 (w), 1472 (w), 1458 (m), 1435 (w), 1423 (m), 1393 (vw), 1364 (w), 1348 (w), 1323 (w), 1304 (w), 1273 (w), 1256 (w), 1242 (w), 1225 (w), 1202 (w), 1184 (w), 1155 (w), 1122 (m), 1092 (vw), 1024 (w), 1005 (vw), 953 (vw), 918 (w), 899 (m), 874 (s), 854 (w), 802 (w), 795 (vw), 779 (vw), 744 (vs), 733 (s), 712 (w), 669 (vw), 635 (w), 623 (m) cm^{-1}. UV/VIS (DCM) λ_{abs} (lg ε): 462 (4.59), 434 (4.47), 418 (4.41), 396 (4.24), 359 (5.05), 349 (4.77), 319 (4.77), 308 (4.76), 287 (4.78), 271 (4.91), 258 (4.92) nm. Fluorescence (DCM) λ_{em} (λ_{ex}): 543, 494 (448) nm. HRMS (LDI-TOF+): *m/z* calcd for $C_{76}H_{52}N_4$ $[M]^+$: 1020.4186; found 1020.4175. Elemental analysis calcd (%) for $C_{76}H_{52}N_4$·0.45 $CHCl_3$: C 85.42, H 4.92, N 5.21. Found: C 85.54, H 4.92, N 4.80.

Synthesis of 10b

In an argon purged 8 mL screw-capped vial extended dione **7** (71 mg, 75 μmol) and 2,3-naphthalenediamine **9** (18 mg, 113 μmol, 1.5 equiv.) were dissolved in chloroform (4.2 mL). After acetic acid (0.25 mL) was added, the reaction mixture was stirred at 70 °C for 19 h. After cooling to rt, the precipitate was collected by filtration and was washed with chloroform (10 mL) and methanol (10 mL) to obtain **10b** as a bright yellow solid (56 mg, 52 μmol, 70%). m.p.: >400 °C. NMR: Due to the low solubility, investigations by NMR-techniques were not possible. UV/VIS (DCM) λ_{abs} (lg ε): 460 (4.61), 433 (4.45), 418 (4.41), 350 (4.94), (336 (4.75)), 303 (4.65), 273 (4.69), 255 (4.72) nm. Fluorescence (DCM) λ_{em} (λ_{ex}): 542, 504 (450) nm. IR (neat, ATR) $\tilde{\nu}$: 2955 (m), 2905 (w), 2868 (w), 1610 (w), 1460 (m), 1425 (m), 1366 (w), 1325 (w), 1275 (w), 1248 (w), 1198 (w), 1186 (w), 1155 (w), 1121 (m), 1094 (w), 1024 (w), 934 (w), 903 (m), 876 (s), 741 (s), 627 (m), 540 (s), 517 (s), 484 (vs), 453 (vs), 432 (vs), 409 (vs) cm^{-1}. HRMS (LDI-TOF+): *m/z* calcd for $C_{80}H_{54}N_4$ $[M]^+$ 1070.4343; found 1070.4332. Elemental analysis calcd (%) for $C_{80}H_{54}N_4$·0.4 DCM: C 87.37, H 5.00, N 5.07. Found: C 87.34, H 5.24, N 5.22.

Synthesis of 12

In a 8 mL screw-capped vial diamine **5** (46 mg, 75 μmol, 1.5 equiv.) and dione **11**[16-17] (31 mg, 50 μmol) were purged with argon for 20 min. The mixture was dissolved in dry THF (4.5 mL) and acetic acid (0.5 mL) was added. The reaction mixture was stirred at 80 °C for 19 h. After cooling to rt, the precipitate was collected by filtration and was washed with methanol (25 mL) to obtain QPP **12** as a bright yellow solid (54 mg, 45 μmol, 90%). m.p.: >400 °C. NMR: Due to the low solubility, investigations by NMR-techniques were not possible. IR (neat, ATR) $\tilde{\nu}$: 3067 (w), 3040 (w), 3020 (w), 2957 (s), 2905 (m), 2868 (w), 1609 (w), 1491 (w), 1474 (m), 1458 (s), 1421 (s), 1394 (w), 1366 (m), 1325 (m), 1302 (w), 1275 (m), 1254 (m), 1223 (w), 1202 (w), 1184 (w), 1155 (m), 1130 (m), 1090 (w), 1024 (w), 934 (w), 918 (w), 901 (m), 881 (m), 797 (w), 764 (w), 741 (vs), 627 (m), 611 (w) cm^{-1}. UV/VIS (THF) λ_{abs} (lg ε): 464 (4.79), 435 (4.62), 419 (4.72), 397 (4.56), 351 (5.15), 319 (4.85) nm. Fluorescence (THF) λ_{em} (λ_{ex}): 538, 493, 473 (380) nm. UV/VIS ($CHCl_3$) λ_{abs} (lg ε): 465 (4.66), 435 (4.54), 421 (4.56), 400 (4.40), 351 (5.06), 321 (4.74), 291 (4.85), 271 (4.85), 261 (4.90) nm. Fluorescence ($CHCl_3$) λ_{em} (λ_{ex}): 540, 491 (392) nm. UV/VIS (DCM) λ_{abs} (lg ε): 465 (4.62), 434 (4.56), 421 (4.54), 401 (4.39), 350 (5.03), 321 (4.75), 290(4.81), 270 (4.91) nm. Fluorescence (DCM) λ_{em} (λ_{ex}): 537, 492 (400) nm. UV/VIS (Toluene) λ_{abs} (lg ε): 467 (4.55), 437 (4.35), 422 (4.38), 398 (4.23), 352 (4.84), 321 (4.52) nm. Fluorescence (Toluene) λ_{em} (λ_{ex}): 529, 483 (392) nm. UV/VIS (Anisole) λ_{abs} (lg ε): 466 (4.68), 438 (4.50), 422 (4.54), 400 (4.38), 353 (5.00), 322 (4.69) nm. Fluorescence (Anisole) λ_{em} (λ_{ex}): 539, 492 (394) nm. HR-MS (MALDI-TOF+, DCTB): *m/z* calcd for $C_{90}H_{60}N_4$ $[M]^+$: 1096.4818; found 1096.4832. Elemental analysis calcd (%) for $C_{94}H_{68}N_4$·THF: C 88.93, H 5.64, N 4.25. Found: C 89.08, H 5.40, N 4.41.

Synthesis of 14

Dinitro compound **3** (202 mg, 300 μmol) was purged with argon for 30 min in an oven dried 25 mL two necked round bottom flask. After dissolving in a 2 : 1 mixture of dry THF (6.6 mL) and dry ethanol (3.3 mL), palladium on charcoal (5 wt%, 64 mg, 30 μmol, 10 mol%) was added in one portion. The mixture was heated to 80 °C, hydrazine monohydrate (0.12 mL, 120 mg, 2.4 mmol, 8 equiv.) was added drop wise and the mixture was stirred for 6 h. The solids were removed by filtration and the solvents were removed from the mother liquor under reduced pressure. The crude brown solid was further purified by column chromatography (SiO_2, DCM, MeOH 2%) to obtain diamine **14** as a beige solid (168 mg, 274 μmol, 91%). m.p.: 265 °C. ^{1}H NMR (600 MHz, THF-d_8, 295 K) δ: 7.35—7.30 (m, 4H, H-10), 7.19—7.14 (m, 4H, H-13), 7.06 (d, *J* = 1.7 Hz, 2H, H-17), 6.96—6.92 (m, 8H, H-11,

H-12), 6.86 (d, J = 7.6 Hz, 2H, H-6), 6.53 (s, 2H, H-2), 6.40 (dd, J = 7.6, 1.7 Hz, 2H, H-5), 5.31 (s, 2H, H-8), 5.09 (s, 2H, H-15), 3.94 (s, 4H, NH_2). ^{13}C NMR (151 MHz, THF-d_8, 295 K) δ: 147.0 (4C, C-9/C-14), 146.9 (4C, C-9/C-14), 145.9 (2C, C-16), 143.5 (2C, C-17), 140.7 (2C, C-4), 135.9 (2C, C-1), 131.7 (2C, C-3), 127.4 (2C, C-5), 126.0 (2C, C-17), 125.7 (4C, C-11/C-12), 125.6 (4C, C-11/C-12), 124.4 (4C, C-13), 124.2 (4C, C-10), 123.4 (2C, C-6), 118.3 (2C, C-2), 55.2 (2C, C-15), 54.8 (2C, C-8). IR (neat, ATR) $\tilde{\nu}$: 3352 (vw), 3331 (vw), 3063 (vw), 3036 (vw), 2957 (w), 2924 (w), 2872 (vw), 2853 (vw), 1624 (w), 1582 (w), 1566 (w), 1524 (w), 1485 (w), 1460 (m), 1412 (w), 1346 (vw), 1306 (vw), 1290 (w), 1269 (w), 1244 (w), 1209 (w), 1182 (w), 1159 (w), 1022 (w), 947 (vw), 924 (vw), 897 (vw), 879 (w), 829 (m), 798 (w), 783 (w), 739 (vs), 669 (w), 656 (w), 638 (w), 623 (s) cm^{-1}. HR-MS (MALDI-TOF+, DCTB ($CHCl_3$)): m/z calcd for $C_{46}H_{32}N_2$ $[M]^+$: 612.2560; found 612.2551. Elemental analysis calcd (%) for $C_{46}H_{32}N_2$·0.5 DCM: C 85.24, H 5.08, N 4.28. Found: C 85.49, H 5.22, N 4.48.

Synthesis of 15

Diamine **14** (306 mg, 495 µmol, 2.2 equiv.) and pyrenetetraone **6** (84 mg, 225 µmol) were dissolved in dry THF (20 mL) and acetic acid (2.5 mL) and were stirred at 80 °C for 16 h. After the reaction was cooled to rt, the mixture was poured into methanol (100 mL). The precipitate was collected by filtration and was washed with methanol (30 mL) and pentane (50 mL) to obtain **15** as a bright yellow solid (273 mg, 179 µmol, 80%). m.p.: >400 °C. ^{1}H NMR (700 MHz, DCM-d_2, 295 K) δ: 9.78 (s, 4H, H-4), 8.37 (s, 4H, H-9), 7.49 (d, J = 1.8 Hz, 4H, H-12), 7.45—7.42 (m, 8H, H-19), 7.32—7.28 (m, 8H, H-16), 7.13 (d, J = 7.5 Hz, 4H, H-23), 7.10—7.05 (m, 16H, H-17, H-18), 6.78 (dd, J = 7.5, 1.8 Hz, 4H, H-24), 5.42 (s, 4H, H-21), 5.28 (s, 4H, H-14), 1.71 (s, 18H, H-1). ^{13}C NMR (176 MHz, DCM-d_2, 295 K) δ: 151.4 (2C, C-3), 145.9 (4C, C-13), 145.7 (8C, C-15/C-20), 145.6 (8C, C-15/C-20), 144.8 (4C, C-22), 143.9 (4C, C-8), 143.6 (4C, C-7), 142.0 (4C, C-10), 137.9 (4C, C-11), 130.7 (4C, C-9), 129.9 (4C, C-5), 127.4 (4C, C-24), 126.0 (2C, C-6), 125.7 (4C, C-12), 125.6 (8C, C-17/C-18), 125.6 (8C, C-17/C-18), 124.9 (4C, C-4), 124.1 (4C, C-16), 123.9 (4C, C-19), 123.3 (4C, C-23), 54.4 (4C, C-14, 54.2 (4C, C-21), 36.2 (2C, C-2), 31.9 (6C, C-1). IR (neat, ATR) $\tilde{\nu}$: 3067 (vw), 3040 (vw), 3020 (vw), 2957 (w), 2868 (vw), 1711 (w), 1609 (vw), 1456 (s), 1420 (w), 1366 (w), 1321 (w), 1290 (w), 1242 (w), 1211 (w), 1192 (w), 1157 (w), 1132 (m), 1022 (w), 932 (vw), 885 (m), 858 (w), 831 (m), 804 (w), 789 (w), 770 (vw), 741 (vs), 665 (w), 644 (vw), 625 (s) cm^{-1}. UV/VIS (DCM) λ_{abs} (lg ε): 438 (4.89), 415 (4.71), 327 (4.93), 287 (4.91), 272 (4.60) nm. Fluorescence (DCM) λ_{em} (λ_{ex}): 456 (423) nm. HR-MS (MALDI-TOF+, DCTB): m/z calcd for $C_{116}H_{78}N_4$ $[M]^+$: 1526.6225; found 1526.6213. Elemental analysis calcd (%) for $C_{116}H_{78}N_4$·0.5 DCM: C 89.10, H 5.07, N 3.57. Found: C 89.20, H 5.11, N 3.68.

Synthesis of 13

In an argon purged 50 mL round bottom flask QPP **15** (76 mg, 50.0 µmol) was dissolved in dry DCM (20 mL). After cooling to 0 °C, trifluoromethane sulfonic acid (150 µL) was added dropwise. DDQ (37 mg, 160 µmol, 3.2 equiv.) was added in one portion and the reaction was stirred at 0 °C for 15 min. The mixture was poured into sat. $NaHCO_3$ aq. solution (100 mL) and was stirred for 2 h. The precipitate was collected by filtration and the phases of the mother liquor were separated. The aqueous phase was extracted with DCM (3 × 75 mL) and the combined organic layer was washed with NaOH solution (1 mol/L, 2 × 150 mL). After drying over $MgSO_4$, the solvent was removed under reduced pressure. The crude solid was combined with the precipitate and was recrystallized from hot THF to obtain **13** (27 mg, 18 µmol, 35%) as a yellow solid. m.p.: >410 °C. ^{1}H NMR (600 MHz, THF-d_8+NaOD, 600 MHz, 295 K) δ: 10.02 (s, 4H, H-4), 9.70 (s, 4H, H-9), 9.16 (s, 4H, H-12), 8.79 (s, 4H, H-23), 7.57—7.49 (m, 16H, H-16, H-19), 7.03 (dd, J = 5.7, 3.0 Hz, 16H, H-17, H-18), 5.92 (s, 4H, H-14), 5.80 (s, 4H, H-21), 1.88 (s, 18H, H-1). The solubility was insufficient to record a ^{13}C NMR spectrum. IR (neat, ATR) $\tilde{\nu}$: 3069 (vw), 3018 (vw), 2964 (w), 2957 (w), 2914 (vw), 2901 (vw), 2862 (vw), 1612 (w), 1495 (w), 1477 (w), 1458 (m), 1421 (m), 1364 (w), 1325 (w), 1302 (vw), 1275 (w), 1256 (w), 1246 (vw), 1204 (w), 1182 (w), 1155 (w), 1132 (m), 1092 (w), 1001 (s), 920 (w), 903 (m), 885 (m), 874 (m), 856 (w), 806 (w), 777 (vw), 743 (vs), 710 (w), 673 (vw), 636 (w), 623 (m), 608 (w) cm^{-1}. UV/VIS (THF) λ_{abs} (lg ε): 467 (4.90), 438 (4.60), 413 (4.22), 355 (5.14), 341 (4.80), 317 (4.70), 302 (4.76) nm. Fluorescence (THF) λ_{em} (λ_{ex}): 539, 493, 473 (434) nm. UV/VIS (DCM) λ_{abs} (lg ε): 467 (4.84), 439 (4.60), 415, 355 (5.13), 341 (4.82), 318 (4.71), 305 (4.76), 270 (4.90) nm. Fluorescence (DCM) λ_{em} (λ_{ex}): 540, 492, 479 (433) nm. UV/VIS (oDCB) λ_{abs} (lg ε): 470 (4.90), 441 (4.61), 358 (5.12), 344 (4.79), 322 (4.69) nm. Fluorescence (oDCB) λ_{em} (λ_{ex}): 542, 508, 491, 481 (439) nm. UV/VIS ($CHCl_3$) λ_{abs} (lg ε): 468 (5.07), 439 (4.82), 413 (4.48), 356 (5.38), 341 (5.04), 320 (4.96), 305 (5.13), 271 (5.06) nm. Fluorescence ($CHCl_3$) λ_{em} (λ_{ex}): 543, 492 (448) nm. UV/VIS (Toluene) λ_{abs} (lg ε): 468 (4.89), 440 (4.62), 416 (4.29), 357 (5.13), 342 (4.83), 342 (4.70) nm. Fluorescence (Toluene) λ_{em} (λ_{ex}): 531, 487, 474 (448) nm. UV/VIS (Anisole) λ_{abs} (lg ε): 469 (4.64), 440 (4.39), 414 (4.03), 358 (4.90), 344 (4.53) nm. Fluorescence (Anisole) λ_{em} (λ_{ex}): 541, 492 (450) nm. UV/VIS (MeCN)* λ_{abs} (lg ε): 473 (4.24), 443 (4.21), 418 (4.16), 357 (4.32), 346 (4.32), 311 (4.27) nm. Fluorescence (MeCN)* λ_{em} (λ_{ex}): 552 (453) nm. UV/VIS (*i*PrOH)* λ_{abs} (lg ε): 474 (4.36), 446 (4.34), 420 (4.42), 358 (4.42), 350 (4.42), 311 (4.36), 278 (4.37) nm. Fluorescence (*i*PrOH)* λ_{em} (λ_{ex}): 547 (425) nm. HRMS (MALDI-TOF+, DCTB): m/z calcd for $C_{116}H_{74}N_4$ $[M]^+$: 1522.5913; found 1522.5914. Elemental analysis calcd (%) for $C_{116}H_{74}N_4$·8.5 DCM: C 66.59, H 4.08, N 2.49. Found: C 66.78, H 4.31, N 2.51.

Supporting Information

The supporting information for this article is available on the WWW under https://doi.org/10.1002/cjoc.202200754.

Acknowledgement

The authors are grateful to "Deutsche Forschungsgemeinschaft" supporting this project (SFB1249 "N-heteropolycyclic compounds as functional materials" TP-A04). The authors acknowledge support by the state of Baden-Württemberg through bwHPC and the German Research Foundation (DFG) through grant no. INST 40/575–1 FUGG (JUSTUS 2 cluster).

References

[1] Stępień, M.; Gońka, E.; Żyła, M.; Sprutta, N. Heterocyclic Nanographenes and Other Polycyclic Heteroaromatic Compounds: Synthetic Routes, Properties, and Applications. *Chem. Rev.* **2017**, *117*, 3479–3716.

[2] Borissov, A.; Maurya, Y. K.; Moshniaha, L.; Wong, W.-S.; Żyła-Karwowska, M.; Stępień, M. Recent Advances in Heterocyclic Nanographenes and Other Polycyclic Heteroaromatic Compounds. *Chem. Rev.* **2022**, *122*, 565–788.

[3] Youn, H.; Park, H. J.; Guo, L. J. Organic Photovoltaic Cells: From Performance Improvement to Manufacturing Processes. *Small* **2015**, *11*, 2228–2246.

[4] Kelley, T. W.; Baude, P. F.; Gerlach, C.; Ender, D. E.; Muyres, D.; Haase, M. A.; Vogel, D. E.; Theiss, S. D. Recent Progress in Organic Electronics: Materials, Devices, and Processes. *Chem. Mater.* **2004**, *16*, 4413–4422.

[5] Anthony, J. E.; Facchetti, A.; Heeney, M.; Marder, S. R.; Zhan, X. n-Type Organic Semiconductors in Organic Electronics. *Adv. Mater.* **2010**, *22*, 3876–3892.

[6] Zhan, X.; Facchetti, A.; Barlow, S.; Marks, T. J.; Ratner, M. A.; Wasielewski, M. R.; Marder, S. R. Rylene and Related Diimides for Organic Electronics. *Adv. Mater.* **2011**, *23*, 268–284.

[7] Kim, K.-H.; Yu, H.; Kang, H.; Kang, D. J.; Cho, C.-H.; Cho, H.-H.; Oh, J.

H.; Kim, B. J. Influence of Intermolecular Interactions of Electron Donating Small Molecules on their Molecular Packing and Performance in Organic Electronic Devices. *J. Mater. Chem. A* **2013**, *1*, 14538–14547.

[8] Fitzner, R.; Elschner, C.; Weil, M.; Uhrich, C.; Körner, C.; Riede, M.; Leo, K.; Pfeiffer, M.; Reinold, E.; Mena-Osteritz, E.; Bäuerle, P. Interrelation between Crystal Packing and Small-Molecule Organic Solar Cell Performance. *Adv. Mater.* **2012**, *24*, 675–680.

[9] Wasserfallen, D.; Kastler, M.; Pisula, W.; Hofer, W. A.; Fogel, Y.; Wang, Z.; Müllen, K. Suppressing Aggregation in a Large Polycyclic Aromatic Hydrocarbon. *J. Am. Chem. Soc.* **2006**, *128*, 1334–1339.

[10] Feng, X.; Wu, J.; Ai, M.; Pisula, W.; Zhi, L.; Rabe, J. P.; Müllen, K. Triangle-Shaped Polycyclic Aromatic Hydrocarbons. *Angew. Chem. Int. Ed.* **2007**, *46*, 3033–3036.

[11] Feng, X.; Pisula, W.; Müllen, K. Large Polycyclic Aromatic Hydrocarbons: Synthesis and Discotic Organization. *Pure Appl. Chem.* **2009**, *81*, 2203–2224.

[12] Wu, D.; Pisula, W.; Haberecht, M. C.; Feng, X.; Müllen, K. Oxygen- and Sulfur-Containing Positively Charged Polycyclic Aromatic Hydrocarbons. *Org. Lett.* **2009**, *11*, 5686–5689.

[13] Gao, B.; Wang, M.; Cheng, Y.; Wang, L.; Jing, X.; Wang, F. Pyrazine-Containing Acene-Type Molecular Ribbons with up to 16 Rectilinearly Arranged Fused Aromatic Rings. *J. Am. Chem. Soc.* **2008**, *130*, 8297–8306.

[14] Kohl, B.; Rominger, F.; Mastalerz, M. Rigid π-Extended Triptycenes via a Hexaketone Precursor. *Org. Lett.* **2014**, *16*, 704–707.

[15] Kohl, B.; Rominger, F.; Mastalerz, M. Crystal Structures of a Molecule Designed Not To Pack Tightly. *Chem. - Eur. J.* **2015**, *21*, 17308–17313.

[16] Kohl, B. *Ph.D. Dissertation*, Ruprecht-Karls Universität, Heidelberg, **2017** (in German).

[17] Kohl, B.; Rominger, F.; Mastalerz, M. A Pyrene-Fused N-Heteroacene with Eleven Rectilinearly Annulated Aromatic Rings. *Angew. Chem. Int. Ed.* **2015**, *54*, 6051–6056.

[18] Ueberricke, L.; Mastalerz, M. Triptycene End-Capping as Strategy in Materials Chemistry to Control Crystal Packing and Increase Solubility. *Chem. Rec.* **2021**, *21*, 558–573.

[19] Baumgärtner, K.; Meza Chincha, A. L.; Dreuw, A.; Rominger, F.; Mastalerz, M. A Conformationally Stable Contorted Hexabenzoovalene. *Angew. Chem. Int. Ed.* **2016**, *55*, 15594–15598.

[20] Baumgärtner, K.; Rominger, F.; Mastalerz, M. Gulf-Selective Postsynthetic Functionalization of a Soluble Hexabenzoovalene. *Chem. - Eur. J.* **2018**, *24*, 8751–8755.

[21] Kohl, B.; Baumgärtner, K.; Rominger, F.; Mastalerz, M. Quinoxalinophenanthrophenazines (QPPs) and Hexabenzoovalenes (HBOs) – Proving the Solubility Enhancement by Triptycene End-Capping. *Eur. J. Org. Chem.* **2019**, 4891–4896.

[22] Ueberricke, L.; Schwarz, J.; Ghalami, F.; Matthiesen, M.; Rominger, F.; Elbert, S. M.; Zaumseil, J.; Elstner, M.; Mastalerz, M. Triptycene End-Capped Benzothienobenzothiophene and Naphthothienobenzothiophene. *Chem. - Eur. J.* **2020**, *26*, 12596–12605.

[23] Wang, X.; Kohl, B.; Rominger, F.; Elbert, S. M.; Mastalerz, M. A Triptycene-Based Enantiopure Bis(Diazadibenzoanthracene) by a Chirality-Assisted Synthesis Approach. *Chem. - Eur. J.* **2020**, *26*, 16036–16042.

[24] Benke, B. P.; Hertwig, L.; Yang, X.; Rominger, F.; Mastalerz, M. Triptycene End-Capped Indigo Derivatives – Turning Insoluble Pigments to Soluble Dyes. *Eur. J. Org. Chem.* **2021**, 72–76.

[25] Yang, X.; Rominger, F.; Mastalerz, M. Benzo-Fused Perylene Oligomers with up to 13 Linearly Annulated Rings. *Angew. Chem. Int. Ed.* **2021**, *60*, 7941–7946.

[26] Yang, X.; Elbert, S. M.; Rominger, F.; Mastalerz, M. A Series of Soluble Thieno-Fused Coronene Nanoribbons of Precise Lengths. *J. Am. Chem. Soc.* **2022**, *144*, 9883–9892.

[27] Shudo, H.; Kuwayama, M.; Segawa, Y.; Itami, K. Synthesis of Cycloiptycenes from Carbon Nanobelts. *Chem. Sci.* **2020**, *11*, 6775–6779.

[28] Kohl, B.; Bohnwagner, M. V.; Rominger, F.; Wadepohl, H.; Dreuw, A.; Mastalerz, M. Attractive Dispersion Interactions Versus Steric Repulsion of *tert*-Butyl groups in the Crystal Packing of a D_{3h}-Symmetric Tris(quinoxalinophenanthrophenazine). *Chem.- Eur. J.* **2016**, *22*, 646–655.

[29] Ueberricke, L.; Holub, D.; Kranz, J.; Rominger, F.; Elstner, M.; Mastalerz, M. Triptycene End-Capped Quinoxalinophenanthrophenazines (QPPs): Influence of Substituents and Conditions on Aggregation in the Solid State. *Chem. - Eur. J.* **2019**, *25*, 11121–11134.

[30] Ueberricke, L.; Wieland, S.; Rominger, F.; Mastalerz, M. Triptycene End-Capped Quinoxalinophenanthrophenazines with Aromatic Substituents – Synthesis, Characterization, and Single-Crystal Structure Analysis. *Org. Mater.* **2019**, *1*, 50–62.

[31] Ueberricke, L.; Ghalami, F.; Zhang, W.-S.; Rao, V.; Rominger, F.; Schröder, R. R.; Elstner, M.; Mastalerz, M. Isostructural Charge-Transfer Cocrystals Based on Triptycene End-Capped Quinoxalinophenanthrophenazine. *Cryst. Growth Des.* **2021**, *21*, 1329–1341.

[32] Müller, M.; Maier, S.; Tverskoy, O.; Rominger, F.; Freudenberg, J.; Bunz, U. H. F. Tetrabenzononacene: "Butterfly Wings" Stabilize the Core. *Angew. Chem. Int. Ed.* **2020**, *59*, 1966–1969.

[33] Müller, M.; Reiss, H.; Tverskoy, O.; Rominger, F.; Freudenberg, J.; Bunz, U. H. F. Stabilization by Benzannulation: Butterfly Azaacenes. *Chem. - Eur. J.* **2018**, *24*, 12801–12805.

[34] Müller, M.; Rüdiger, E. C.; Koser, S.; Tverskoy, O.; Rominger, F.; Hinkel, F.; Freudenberg, J.; Bunz, U. H. F. "Butterfly Wings" Stabilize Heptacene. *Chem. - Eur. J.* **2018**, *24*, 8087–8091.

[35] Rüdiger, E. C.; Müller, M.; Freudenberg, J.; Bunz, U. H. F. Starphenes and Phenes: Structures and Properties. *Org. Mater.* **2019**, *01*, 1–18.

[36] Chen, W.; Yu, F.; Xu, Q.; Zhou, G.; Zhang, Q. Recent Progress in High Linearly Fused Polycyclic Conjugated Hydrocarbons (PCHs, $n > 6$) with Well-Defined Structures. *Adv. Sci.* **2020**, *7*, 1903766.

[37] Voll, C.-C. A.; Markopoulos, G.; Wu, T. C.; Welborn, M.; Engelhart, J. U.; Rochat, S.; Han, G. G. D.; Sazama, G. T.; Lin, T.-A.; Van Voorhis, T.; Baldo, M. A.; Swager, T. M. Lock-and-Key Exciplexes for Thermally Activated Delayed Fluorescence. *Org. Mater.* **2020**, *2*, 1–10.

[38] Reinhard, D.; Rominger, F.; Mastalerz, M. Synthesis of Triphenylene-Based Triptycenes via Suzuki–Miyaura Cross-Coupling and Subsequent Scholl Reaction. *J. Org. Chem.* **2015**, *80*, 9342–9348.

[39] Ma, L.; Hu, Q.-S.; Vitharana, D.; Wu, C.; Kwan, C. M. S.; Pu, L. A New Class of Chiral Conjugated Polymers with a Propeller-Like Structure. *Macromolecules* **1997**, *30*, 204–218.

[40] Hu, J.; Zhang, D.; Harris, F. W. Ruthenium(III) Chloride Catalyzed Oxidation of Pyrene and 2,7-Disubstitued Pyrenes: An Efficient, One-Step Synthesis of Pyrene-4,5-diones and Pyrene-4,5,9,10-tetraones. *J. Org. Chem.* **2005**, *70*, 707–708.

[41] Hesse, M.; Meier, H.; Zeeh, B. *Spektroskopische Methoden in der organischen Chemie*, Thieme, Stuttgart, **2005** (in German).

[42] Ueberricke, L.; Mizioch, D.; Ghalami, F.; Mildner, F.; Rominger, F.; Oeser, T.; Elstner, M.; Mastalerz, M. Quinoxalinophenanthrophenazine Based Cruciforms. *Eur. J. Org. Chem.* **2021**, 4816–4823.

[43] Ueberricke, L.; Ciubotaru, I.; Ghalami, F.; Mildner, F.; Rominger, F.; Elstner, M.; Mastalerz, M. Di- and Tetracyano-Substituted Pyrene-Fused Pyrazaacenes: Aggregation in the Solid State. *Chem. - Eur. J.* **2020**, *26*, 11634–11642.

[44] Kasha, M.; Rawls, H. R.; Ashraf El-Bayoumi, M. The Exciton Model in Molecular Spectroscopy. *Pure Appl. Chem.* **1965**, *11*, 371–392.

[45] Bordas-Nagy, J.; Jennings, K. R. Collision-Induced Decomposition of Ions. *Int. J. Mass Spectrom. Ion Processes* **1990**, *100*, 105–131.

[46] Sheldrick, G. M. Crystal Structure Refinement with SHELXL. *Acta Crystallogr., Sect. C: Struct. Chem.* **2015**, *71*, 3–8.

[47] Troisi, A.; Orlandi, G. Dynamics of the Intermolecular Transfer Integral in Crystalline Organic Semiconductors. *J. Phys. Chem. A* **2006**, *110*, 4065–4070.

[48] Kubas, A.; Hoffmann, F.; Heck, A.; Oberhofer, H.; Elstner, M.; Blumberger, J. Electronic Couplings for Molecular Charge Transfer: Benchmarking CDFT, FODFT, and FODFTB against High-Level *ab initio* Calculations. *J. Phys. Chem.* **2014**, *140*, 104105.

[49] Halder, M.; Datta, S.; Bolel, P.; Mahapatra, N.; Panja, S.; Vardhan, H.; Kayal, S.; Khatua, D. K.; Das, I. Reorganization Energy and Stokes Shift Calculations from Spectral Data as New Efficient Approaches in Dis-

tinguishing the End Point of Micellization/Aggregation. *Anal. Methods* **2016**, *8*, 2805–2811.
[50] Gavezzotti, A. Are Crystal Structures Predictable? *Acc. Chem. Res.* **1994**, *27*, 309–314.
[51] Gavezzotti, A.; Filippini, G. Geometry of the Intermolecular X-H···Y (X, Y = N, O) Hydrogen Bond and the Calibration of Empirical Hydrogen-Bond Potentials. *J. Phys. Chem.* **1994**, *98*, 4831–4837.
[52] Yoshizawa, M.; Catti, L. Bent Anthracene Dimers as Versatile Building Blocks for Supramolecular Capsules. *Acc. Chem. Res.* **2019**, *52*, 2392–2404.

Manuscript received: November 18, 2022
Manuscript revised: December 22, 2022
Manuscript accepted: December 28, 2022
Accepted manuscript online: December 29, 2022
Version of record online: March 22, 2023

The Authors